Thermal Conversion of Biomass: Comprehensive Reactor and Particle Modeling

Johann C. Wurzenberger, Susanne Wallner, and Harald Raupenstrauch
Institut für Apparatebau, Mechanische Verfahrenstechnik und Feuerungstechnik,
Technische Universität Graz, A-8010 Graz, Austria

Johannes G. Khinast
Dept. of Chemical and Biochemical Engineering, Rutgers University, Piscataway, NJ 08854

Thermal conversion of biomass is often carried out in packed-bed furnaces. Optimization of thermal efficiency and furnace emissions is an important goal, which requires accurate understanding of all physical and chemical effects in the reactor. A combined transient single particle and fuel-bed model is presented. The fuel-bed model is discretized, and a representative particle is chosen and discretized in a radial direction at each grid point. Mass, momentum and energy balances are solved for the entire system. Drying is modeled using an equilibrium approach, and primary pyrolysis is described by independent parallel-reactions. Secondary tar cracking, homogeneous gas reactions, and heterogeneous char reactions are modeled using kinetic data from literature. Simulations validated for single particles agree well with experimental studies. Simulation results for the combustion of a biomass bed are presented for one set of furnace conditions.

Introduction

Biomass, such as wood, bark, straw, or biowaste is becoming an increasingly important energy source of the future. Considering the decreasing resources of fossil fuels and their effect on global warming, CO_2-neutral biomass is a promising alternative. In 2000 biomass provided about 4% of all U.S. primary energy and has an estimated potential of up to 20% (American Bioenergy Association, 2000). In the EU, biomass covers about 3% (Finland 18%, France 0.8%) of the primary energy (EuroREX, 2000; Hall and House, 1995), and the EU targets to increase its use to 12% by 2010 (European Commission, 1997).

In the past years, many research groups studied the feasibility of biomass conversion for energy production. For example, technical and economic aspects of biomass gasification systems were discussed in great detail by Bridgwater (1995), who compared costs, fuel pre-treatment, gasification efficiency, and electricity production of several plants. Van den Broek et al. (1996) presented an overview of the state-of-the-art combustion technologies, effectiveness, and investment costs of biomass plants. Beenackers (1999) gave an overview of commercially used down-and-up-draft biomass gasifiers.

Currently, biomass is used either in gasification or combustion systems. Gasification reactions are endothermic reactions of fuel with H_2O or CO_2, while combustion involves exothermic reactions between fuel and oxygen. Typically, both classes of reactions occur simultaneously, and the difference between gasification and combustion is determined by the amount of oxygen supplied. Combustors, which operate under overstoichiometric conditions, are mostly used in small furnaces for heating purposes of residential buildings (< 20 kW) or districts (< 5 MW). The main products of combustion are H_2O and CO_2. Gasifiers are supplied with an understoichiometric amount of oxygen in order to maintain autothermic operation conditions. Gasifiers are often used for the production of steam and electrical power. The primary product is gas rich in H_2, CO, and hydrocarbons. In large-scale plants (> 10 MW) this gas is used in turbines or is co-combusted in coal-fired furnaces. In small-scale gasifiers, the product gas can be utilized in gas motors or fuel cells.

Biomass gasification or combustion is performed in many different types of furnaces, such as, fixed and moving bed

Correspondence concerning this article should be addressed to J. C. Wurzenberger.

reactors, fluidized or circulating fluidized beds, as well as pulverized fuel burners. The decision concerning the type of furnace is made on the basis of fuel characteristics (such as particle size, particle-size distribution, moisture, and ash content), fuel feed rate, and desired products. Fixed or moving bed furnaces are distinguished according to fuel and gas flow patterns (Hobbs et al., 1992). Furnaces with co- or countercurrent operation are limited by the particle-size distribution and by the resulting pressure drop in the bed. Compared to cocurrent operations, countercurrent operation generates a rather cold gas with a higher amount of tar. For coarse particle-size distributions, crosscurrent furnaces are used in which the fuel is transported through the furnace by a moving grate. In different regions of the grate, the air supply can be adjusted, which enables a highly flexible operation. One advantage of fluidized beds is the good mass and heat transfer between gas and the individual particles (Neogi et al., 1986). The bed usually consists of carrier materials (such as sand) with high heat capacities, which stabilize changes in the fuel composition (such as moisture) and system temperature. Additional materials, such as dolomite, may be used to catalytically improve the decomposition of tar (Rapagna et al., 2000). Thus, this reactor type is often used for the combustion or gasification of high-ash wood-wastes or slow burning chars (Dry and La Nauze, 1980). Pulverized fuel burners have so-called suspension firing, in which solid fuel and air are mixed and injected together into the furnace chamber (Govind and Shah, 1984). This technique requires intensive fuel pretreatment, but shows high thermal efficiency and flexibility with regard to operating conditions (Schwleger, 1980).

In order to optimize the thermal efficiency and to predict product gas composition, numerous mathematical models for biomass conversion systems were developed. Bryden and Ragland (1995) described the combustion of whole trees using a one-dimensional (1-D), steady-state model in an updraft fixed-bed combustor, which accounts for drying, pyrolysis, and other reactions. Fixed-bed biomass drying was investigated by Raupenstrauch (1991) using a transient 2-D model. A heterogeneous, 1-D, transient model of the gasification of biomass was presented by Di Blasi (2000). It was shown that gas-phase combustion and primary pyrolysis are important for the stabilization of the reaction front, which underlines the need for comprehensive modeling of these effects. Cooper and Hallet (2000) showed the importance of heterogeneous models in their investigation of packed-bed combustion of char, since substantial temperature differences arise between the gas and solid phase in the oxidation zones. Ignition front temperature and front velocity of moving-bed straw combustors were modeled by Van der Lans et al. (2000). It was shown that the front velocity, as a function of the air to fuel ratio, was mainly affected by the supplied air, the radiative heat transport in the bed, and the fuel moisture. The impact of co- and countercurrent primary air supply and fuel bed mixing on the ignition behavior and front velocity was, for example, investigated by Amundson and Arri (1978) and Hartner (1996). Simpler models for the estimation of the ignition front velocity were presented by Saastamoinen et al. (2000) and Thunmann and Leckner (2000).

The present work focuses on the gasification/combustion of biomass in crosscurrent moving beds. The fuel conversion takes place by various mechanisms, that is, drying, primary pyrolysis, secondary tar cracking, gasification, and combustion. During drying, fuel moisture evaporates followed by pyrolysis, which is the thermal decomposition of the solid fuel that forms gases, tar, and solid char residues. In addition to pyrolysis, thermal cracking of tar occurs. Gasification comprises a complex set of heterogeneous reactions between CO_2, H_2O, and the solid char. The heat required for drying, pyrolysis, and gasification is generated by the exothermic reactions of O_2 with char and combustible gas components. All effects occur simultaneously, and detailed modeling is necessary in order to simulate the behavior of the entire fuel bed. An essential simplification in all of the above-cited investigations was the assumption of isothermal particles. In the case of large biomass particles, however, the processes are strongly controlled by heat and mass transfer inside the particle, and the production of volatiles is a function of the rates of heat transfer (Bliek et al., 1966). The composition of the pyrolysis gases is influenced by the intraparticle mass transfer, since longer residence times change the extent of secondary cracking. Thus, a comprehensive approach to studying large particles and fast heating rates, as they occur in biomass furnaces, requires a detailed single-particle model combined with a packed-bed reactor model.

The specific objective of this article is twofold. First, simulations of single particles, decoupled from the packed bed model, are performed. These simulations are compared with experimental investigations and show the validity of the chosen overall approach for drying, pyrolysis, gasification, and combustion. Second, operation conditions of a moving bed combustor are chosen, and the combined packed-bed and single-particle model are used to predict the overall behavior of this system.

Model

A moving bed furnace is shown in Figure 1. The fuel enters the furnace on the lefthand side and migrates through it. Under constant operating conditions, a pseudo-steady state develops. Provided that local gradients in the x-direction can be neglected, a transient 1-D model (in the flow direction z of the primary air) can be used to describe the entire fuel bed. This is typically true for moving bed furnaces, and this approach has been widely used in literature (for example, Van der Lans et al., 2000; Shin and Choi, 2000). Using the migration velocity of the bed, time can be transformed into the coordinate x in direction of the grate.

Transient 1-D models of the packed-bed reactors have been used by a large number of researchers including Liu and

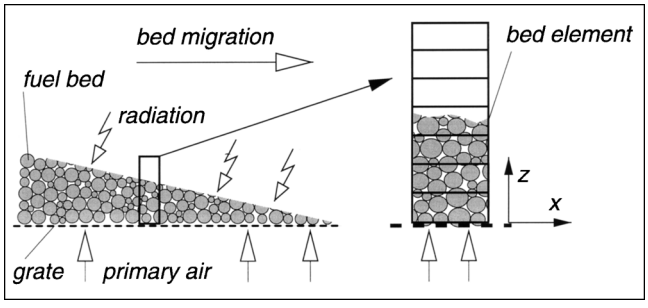

Figure 1. Moving bed furnace.

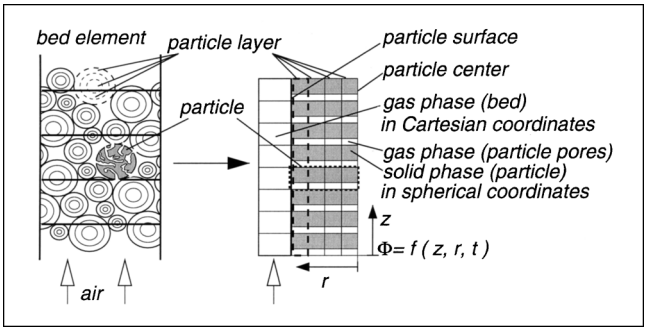

Figure 2. Discretization scheme.

At each grid point of the 1-D bed model (direction of the primary air), one representative particle is chosen and discretized over its radius.

Amundson (1962), Eigenberger (1972), Shin and Choi (2000), and Di Blasi (2000). In all these models, solid particles are considered to be small enough to be isothermal (Bryden and Ragland, 1995). The fact that the particles are porous and that reactions take place within this structure is taken into account using effectiveness-factors (for example, Stillman, 1979).

The model presented here considers gradients both in the bed and inside single particles. As shown in Figure 2, in each cell of the discretization in the z-direction one representative particle is chosen and discretized in the radial direction. Thus, the entire bed is divided into two subsystems, that is, the gas phase inside the bed and the individual particles. This approach is called a "transient 1-D + 1-D model." The gas phase within the packed bed is described by 1-D Cartesian coordinates, and the individual particles by 1-D spherical coordinates. Dieterich (1998) used this concept to simulate systems of catalytic packed beds, and Chejne et al. (2000) for the modeling of coal combustion in stacks.

Our model takes into account heatup, drying, pyrolysis, secondary tar cracking, homogeneous gas reactions, and heterogeneous combustion/gasification reactions. In the gas-phase eight species (O_2, N_2, CO, CO_2, H_2, H_2O, CH_4 and tar) are considered. The solid phase is beech.

Gas phase in the packed bed

The continuity equation of the gas phase in the packed bed is

$$\frac{\partial \epsilon_{g,\mathrm{bed}}\,\rho_{g,\mathrm{bed}}}{\partial t} = -\frac{\partial \epsilon_{g,\mathrm{bed}}\,\rho_{g,\mathrm{bed}} v_{g,\mathrm{bed}}}{\partial z} + \alpha_{\mathrm{par}}\dot{m}_{\mathrm{par}} \qquad (1)$$

where $\rho_{g,\mathrm{bed}}$ is the density of the gas phase, $v_{g,\mathrm{bed}}$ is the gas velocity, and $\epsilon_{g,\mathrm{bed}}$ is the porosity of the bed. The term $a_{\mathrm{par}}\dot{m}_{\mathrm{par}}$ denotes the mass exchange between the gas phase of the bed and single particles. The pressure drop in the bed is described by the Ergun-equation (Ergun, 1952)

$$0 = \frac{dp_{g,\mathrm{bed}}}{dz} - A_E v_{g,\mathrm{bed}} - B_E v_{g,\mathrm{bed}} |v_{g,\mathrm{bed}}| \qquad (2)$$

where $p_{g,\mathrm{bed}}$ is the system pressure and A_E, B_E are model parameters. The species conservation equation is given by

$$\begin{aligned}\epsilon_{g,\mathrm{bed}}\,\rho_{g,\mathrm{bed}}\frac{\partial w_{j,g,\mathrm{bed}}}{\partial t} &= -\epsilon_{g,\mathrm{bed}}\,\rho_{g,\mathrm{bed}} v_{g,\mathrm{bed}}\frac{\partial w_{j,g,\mathrm{bed}}}{\partial z} \\ &+ \frac{\partial}{\partial z}\left(\epsilon_{g,\mathrm{bed}}\,\rho_{g,\mathrm{bed}} D_{\mathrm{eff,bed}}\frac{\partial w_{j,g,\mathrm{bed}}}{\partial z}\right) \\ &+ a_{\mathrm{par}}\left(\dot{m}_{j,\mathrm{par}} - w_{j,g,\mathrm{bed}}\dot{m}_{\mathrm{par}}\right) \\ &+ \epsilon_{g,\mathrm{bed}} MG_j \sum_i^{R_{\mathrm{hom}}} \nu_{i,j,\mathrm{hom}}\dot{r}_{i,\mathrm{hom}} \qquad (3)\end{aligned}$$

$w_{j,g,\mathrm{bed}}$ is the mass fraction of species j, $D_{\mathrm{eff,bed}}$ is an effective diffusion coefficient, and $\dot{m}_{\mathrm{par}}$, $\dot{m}_{j,\mathrm{par}}$ are the total and the species mass fluxes leaving the particles. $\dot{r}_{i,\mathrm{hom}}$ represents the molar reaction rate of the homogeneous gas reactions (including tar cracking) with stoichiometric coefficients $\nu_{i,j,\mathrm{hom}}$. The energy balance is

$$\begin{aligned}&\epsilon_{g,\mathrm{bed}}\,\rho_{g,\mathrm{bed}} c_{p,g,\mathrm{bed}}\frac{\partial T_{g,\mathrm{bed}}}{\partial t} - \frac{\partial \epsilon_{g,\mathrm{bed}}\,p_{g,\mathrm{bed}}}{\partial t} \\ &= -\epsilon_{g,\mathrm{bed}}\,\rho_{g,\mathrm{bed}} c_{p,g,\mathrm{bed}} v_{g,\mathrm{bed}}\frac{\partial T_{g,\mathrm{bed}}}{\partial z} \\ &+ \epsilon_{g,\mathrm{bed}}\lambda_{\mathrm{eff,bed}}\frac{\partial^2 T_{g,\mathrm{bed}}}{\partial z^2} + \epsilon_{g,\mathrm{bed}}\,\rho_{g,\mathrm{bed}} D_{\mathrm{eff,bed}} \\ &\times \sum_j^S \frac{\partial h_{j,g,\mathrm{bed}}}{\partial z}\frac{\partial w_{j,g,\mathrm{bed}}}{\partial z} \\ &+ a_{\mathrm{par}}\left(\sum_j^S \dot{m}_{j,\mathrm{par}}\left(h_{j,g,\mathrm{par}} - h_{j,g,\mathrm{bed}}\right) + \lambda_{\mathrm{eff,par}}\left.\frac{\partial T_{\mathrm{par}}}{\partial r}\right|_{r=R}\right) \\ &+ \epsilon_{g,\mathrm{bed}}\sum_i^{R_{\mathrm{hom}}}\left(-\Delta h_{i,\mathrm{hom}}\right)\dot{r}_{i,\mathrm{hom}} \qquad (4)\end{aligned}$$

where $T_{g,\mathrm{bed}}$ is the gas temperature, $\lambda_{\mathrm{eff,bed}}$ is the effective heat conductivity of the entire bed, and h_j is the enthalpy of component j. The heat exchange with the particles occurs by convection $\dot{m}_{j,\mathrm{par}}\,(h_{j,g,\mathrm{par}} - h_{j,g,\mathrm{bed}})$, and conduction $\lambda_{\mathrm{eff,par}}\,\partial T_{\mathrm{par}}/\partial r|_{r=R}$ at the particle surface. Homogeneous gas-phase reactions with reaction enthalpies $\Delta h_{i,\mathrm{hom}}$ are considered.

The second term in the lefthand side of this equation (and also of Eq. 8) and the third term on the righthand side represent the pressure volume work and the enthalpy transport due to species diffusion, respectively. Both terms are negligible in the present application, but are mentioned in the model equations for the sake of completeness.

Single particle

The conservation equations of the gas phase in the pore system of single particles are similar to Eqs. 1–4, but are written in spherical coordinates (Eqs. 5–8). Here, Darcy's law (Kaviany, 1991) is used. In the species conservation equations $\tilde{\nu}_{i,j,\mathrm{het}}$ is a mass specific stoichiometric coefficient, and $\dot{r}_{i,\mathrm{het}}$ denotes the rates of heterogeneous reactions.

$$\frac{\partial}{\partial t}\left[\left(1-\epsilon_{g,\mathrm{bed}}\right)\epsilon_g\,\rho_g\right] = -\frac{1}{r^2}\frac{\partial}{\partial r}\left[r^2\left(1-\epsilon_{g,\mathrm{bed}}\right)\epsilon_g\,\rho_g v_g\right] + \left(1-\epsilon_{g,\mathrm{bed}}\right)\sum_i^{R_{\mathrm{het}}}\tilde{\nu}_{i,j,\mathrm{het}}\dot{r}_{i,\mathrm{het}} \quad (5)$$

$$0 = \frac{dp_g}{dr} + \frac{\eta}{C_D}v_g \quad (6)$$

$$\left(1-\epsilon_{g,\mathrm{bed}}\right)\epsilon_g\,\rho_g\frac{\partial w_{j,g}}{\partial t} = -\left(1-\epsilon_{g,\mathrm{bed}}\right)\epsilon_g\,\rho_g v_g\frac{\partial w_{j,g}}{\partial r} + \frac{1}{r^2}\frac{\partial}{\partial r}\left[r^2\left(1-\epsilon_{g,\mathrm{bed}}\right)\epsilon_g\,\rho_g D_{\mathrm{eff,par}}\frac{\partial w_{j,g}}{\partial r}\right] + \left(1-\epsilon_{g,\mathrm{bed}}\right)\left[\epsilon_g MG_j\sum_i^{R_{\mathrm{hom}}}\nu_{i,j,\mathrm{hom}}\dot{r}_{i,\mathrm{hom}} + \sum_i^{R_{\mathrm{het}}}\left(\tilde{\nu}_{i,j,\mathrm{het}}\dot{r}_{i,\mathrm{het}} - w_{j,g}\sum_j^{S}\tilde{\nu}_{i,j,\mathrm{het}}\dot{r}_{i,\mathrm{het}}\right)\right] \quad (7)$$

Under the assumption that gas, liquid, and solid phase in the particle have the same local temperature, only one overall energy equation is required

$$\left(1-\epsilon_{g,\mathrm{bed}}\right)\rho_{\mathrm{par}}c_{p,\mathrm{par}}\frac{\partial T_{\mathrm{par}}}{\partial t} - \frac{\partial}{\partial t}\left[\left(1-\epsilon_{g,\mathrm{bed}}\right)p_{\mathrm{par}}\right] = -\left(1-\epsilon_{g,\mathrm{bed}}\right)\epsilon_g\,\rho_g c_{p,g}v_g\frac{\partial T_{\mathrm{par}}}{\partial r} + \frac{1}{r^2}\frac{\partial}{\partial r}\left(r^2\left(1-\epsilon_{g,\mathrm{bed}}\right)\lambda_{\mathrm{eff,par}}\frac{\partial T_{\mathrm{par}}}{\partial r}\right) + \left(1-\epsilon_{g,\mathrm{bed}}\right)\epsilon_g\,\rho_g D_{\mathrm{eff,par}}\times\sum_j^{S}\frac{\partial h_{j,g\,\mathrm{par}}}{\partial r}\frac{\partial w_{j,g}}{\partial r} + \left(1-\epsilon_{g,\mathrm{bed}}\right)\times\left[\sum_i^{R_{\mathrm{hom}}}\left(-\Delta h_{i,\mathrm{hom}}\right)\dot{r}_{i,\mathrm{hom}} + \sum_i^{R_{\mathrm{het}}}\left(-\Delta h_{i,\mathrm{het}}\right)\dot{r}_{i,\mathrm{het}}\right] + \left(1-\epsilon_{g,\mathrm{bed}}\right)\frac{\partial}{\partial z}\left(\lambda_{\mathrm{eff,bed}}\frac{\partial T_{\mathrm{par}}(z,r=R,t)}{\partial z}\right) \quad (8)$$

T_{par} is the local particle temperature, $c_{p,\mathrm{par}}$ is the overall heat capacity of the particle, and $\lambda_{\mathrm{eff,par}}$ is the overall heat conductivity. The heats of the homogeneous and heterogeneous reactions are $\Delta h_{i,\mathrm{hom}}$ and $\Delta h_{i,\mathrm{het}}$, respectively. The last term on the righthand side of this equation takes into account a conductive heat transport between the surfaces of the particles at different bed heights. Total mass and species balances of the solid and liquid in the particle are

$$\frac{d}{dt}\left[\left(1-\epsilon_{g,\mathrm{bed}}\right)\epsilon_s\,\rho_s\right] = \left(1-\epsilon_{g,\mathrm{bed}}\right)\sum_i^{R_{\mathrm{het}}}\tilde{\nu}_{i,j,\mathrm{het}}\dot{r}_{i,\mathrm{het}} \quad (9)$$

$$\frac{d}{dt}\left[\left(1-\epsilon_{g,\mathrm{bed}}\right)\epsilon_l\,\rho_l\right] = \left(1-\epsilon_{g,\mathrm{bed}}\right)\sum_i^{R_{\mathrm{het}}}\tilde{\nu}_{i,j,\mathrm{het}}\dot{r}_{i,\mathrm{het}} \quad (10)$$

Table 1. Primary Pyrolysis Kinetics of Beech*

No.	Component	$k_{0,j}$ (1/s)	E_j (kJ/mol)	$w_{s,\max,j}$ (kg/kg d.b.)
1	H_2O	3.68×10^{13}	149.5	0.0480
2	CO	9.00×10^{9}	111.0	0.0506
3	CO_2	5.23×10^{9}	105.0	0.0724
4	H_2	4.73×10^{4}	92.5	0.0060
5	CH_4	1.09×10^{5}	71.3	0.0106
6	tar	2.09×10^{10}	112.7	0.6340

*TGA-experiments with 1 mm particles under atmospheric conditions, at a heating rate of 5 K/min and a maximum temperature of 1,173 K (Seebauer, 1999).

ρ_s (ρ_l) are the densities of the solid (liquid), and ϵ_s (ϵ_l) are the corresponding volume fractions. The solid structure of wood decomposes during pyrolysis into several gaseous components and solid char. The maximum yields of different pyrolysis products (see Table 1) are experimentally determined and can be used to simplify the calculation of the changing solid composition. Initially, wood is represented by the maximum yield of different pyrolysis gases, char, and ashes (Figure 3).

For each of these components, one solid-phase mass balance is written

$$\left(1-\epsilon_{g,\mathrm{bed}}\right)\epsilon_s\,\rho_s\frac{dw_{j,s}}{dt} = \left(1-\epsilon_{g,\mathrm{bed}}\right)\sum_i^{R_{\mathrm{het}}}\left(\tilde{\nu}_{i,j,\mathrm{het}}\dot{r}_{i,\mathrm{het}} - w_{j,g}\sum_j^{S}\tilde{\nu}_{i,j,\mathrm{het}}\dot{r}_{i,j,\mathrm{het}}\right) \quad (11)$$

where $w_{j,s}$ is the mass fraction of solid species. The "solid volatiles" decomposition is described by pyrolysis kinetics, and char is consumed by heterogeneous reactions.

Initial and boundary conditions are chosen according to the specific application. In a general notion, the boundary condi-

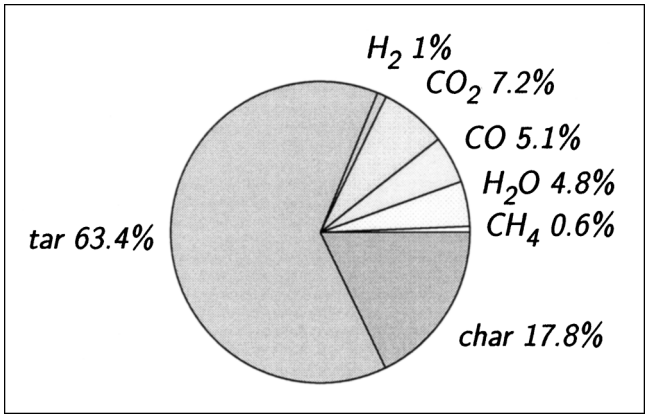

Figure 3. Maximum yields of pyrolysis products.

tions of the individual particles are

$$\rho\epsilon\upsilon\Phi_{\text{par}}\big|_{r=R^-} - \Gamma\frac{\partial\Phi_{\text{par}}}{\partial r}\bigg|_{r=R^-} = \rho\epsilon\upsilon\Phi_{\text{par}}\big|_{r=R^+} + \kappa\left[\Phi_{\text{par}}\big|_{r=R^+} - \Phi_{\text{bed}}\right] \quad (12)$$

where Φ is a general conservation variable, Γ represents the dispersion coefficient or the heat conductivity, and κ is a general transfer coefficient.

Equations 1–12 are a system of partial differential equations (PDEs), ordinary differential equations (ODEs), and algebraic equations (AEs). All AEs and spatial ODEs (that is, the Ergun equation and Darcy's law) are substituted into the PDEs, and a system consisting of PDEs and ODEs (that is, mass balances of the solid phase) is obtained. The PDEs are discretized in space using the method of finite volumes. The resulting system of stiff ODEs is then solved using LIMEX (Deuflhard et al., 1987). Validation simulations showed that 20 gridpoints are sufficient for the discretization of the particles. For the bed discretization, the same number of gridpoints gave sufficient accuracy. The computation time for single-particle simulations is in the range of several minutes on a Compaq XP1000. Simulations of entire beds required CPU times between several hours and one day, depending on the number of gridpoints and on the considered simulation task.

Drying

Biomass typically has a water content of about 40–100% d.b. (dry basis) and, therefore, an accurate description of drying is essential in combustion/gasification processes. Factors impacting the drying process are particle size, initial moisture content, temperature, relative humidity, and velocity of the surrounding gas (Sasstamoinen et al., 1995). Cenkowski et al. (1993) reviewed different "grain drying" models in packed beds. The models are classified into nonequilibrium, equilibrium, and logarithmic type. In this study, an equilibrium model is used, that is, the liquid (free and absorbed water) is considered to be in equilibrium with the local gas phase in the pores. Numerically, this can be achieved by assuming a drying rate

$$\dot{r}_{\text{dry}} = -k_0\epsilon_g\cdot\left(\frac{p^*_{\text{H}_2\text{O}}}{RT_{\text{par}}} - \frac{w_{g,\text{H}_2\text{O}}\rho_g}{MG_{\text{H}_2\text{O}}}\right) \quad (13)$$

with a very large rate constant k_0. Thus, the gas-phase vapor concentration is always in equilibrium with the liquid phase. The equilibrium pressure of water $p^*_{\text{H}_2\text{O}}$ is the saturation pressure $p^S_{\text{H}_2\text{O}}$ multiplied with a correction function φ (c_l, T_{par}) (Eq. 14). When the moisture content c_1 is less than that of the fiber saturation point c_{FSP} of the solid, φ reduces the saturation pressure. The vapor pressure $p^S_{\text{H}_2\text{O}}$ is calculated using the Antoine equation

$$c_1 \le c_{\text{FSP}}: \quad p^*_{\text{H}_2\text{O}} = p^S_{\text{H}_2\text{O}}\varphi(c_l, T_{\text{par}})$$
$$c_l \ge c_{\text{FSP}}: \quad p^*_{\text{H}_2\text{O}} = p^S_{\text{H}_2\text{O}} \quad (14)$$

A detailed description of the function φ is given by Rummer (1998).

Primary pyrolysis

The nonoxidative decomposition of biomass, called pyrolysis, has a strong influence on the entire gasification/combustion process, since the amount of volatiles can be up to 80% of the entire solid mass. In the first step, the *primary pyrolysis*, the solid phase thermally decomposes into gases, tar, and char. The conversion of tar into gas and char is summarized as *second pyrolysis* (Di Blasi, 1993). In the literature several pyrolysis models for wood were proposed. Van Krevelen (1981) assumed the existence of metaplast and semi-char as intermediate products and developed a complex model that considers competing and consecutive reactions. Liliedahl and Sjöström (1994) presented an empirical model for isothermal decomposition. A simplified approach was used by Winter (1997), who assumed that the formation of all volatiles is equal, thus, describing the formation of individual components with one single rate equation. Alves and Figueiredo (1989) and Antal et al. (1980) used the approach of independent parallel reactions. This model is also utilized in this study and can be described by

$$\text{C}_x\text{H}_y\text{O}_z \xrightarrow{k_j} \text{Product}_{j=[\text{H}_2\text{O}(g),\text{CO}(g),\text{CO}_2(g),\text{H}_2(g),\text{CH}_4(g)\text{tar}(g),\text{char}(s)]} \quad (15)$$

where each product j is formed according to an independent rate expression. Mass loss of the solid is described by irreversible reactions of first order, where the activation energies E_j are assumed to be different for each species (Pitt, 1962). Thus, the individual pyrolysis rates $\dot{r}_{\text{pyro},j}$ (kg/m^3/s) are given by

$$\dot{r}_{\text{pyro},j} = k_{0,j}\cdot\exp^{(-E_j/RT_{\text{par}})}\cdot(w_{j,s}\rho_s\epsilon_s) \quad (16)$$

The term $w_{j,s}\rho_s\epsilon_s$ is the amount of not volatilized pyrolysis gas left in the solid phase. The reaction stops when a species has reached its specific maximum degree of devolatilization. The kinetic parameters used in this study are taken from thermogravimetric (TGA) measurements and are shown in Table 1.

The heat of wood pyrolysis is relatively small and was investigated by Rath et al. (2002b), who report a variability of heat of reaction depending on the wood, the particle size, and the final char yield. For beech, this heat of pyrolysis ranges from 150 kJ/kg d.b. at a final char yield of about 0.18 kg/kg d.b. to -150 kJ/kg d.b. at a final char yield of 0.25 kg/kg d.b. An explanation of the changing heat of reaction may be the simultaneous occurrence of exothermic primary char production and endothermic formation of volatiles. In this work a heat-neutral primary pyrolysis model was used.

Secondary pyrolysis

Primary pyrolysis is followed by secondary cracking of tar, which is a mixture of condensed hydrocarbons (Kalson and Briggs, 1985). Crack reactions occur homogeneously in the

Table 2. Relative Yields of Tar Cracking Products (Boroson and Howard, 1989)

Component	$\tilde{\nu}_j$	Component	$\tilde{\nu}_j$
CO	0.78×0.72222	CO_2	0.78×0.14222
H_2	0.78×0.02222	CH_4	0.78×0.11334
tar	-1.00000	tar_{inert}	0.22

gas phase or heterogeneously at the surface of the biomass or char particles. In the present study, tar cracking is considered to follow an overall reaction, as given in Eq. 17. Higher aliphates, such as ethane, ethene, or propene are lumped into methane formation

$$\text{tar} \rightarrow \tilde{\nu}_{CO}CO(g) + \tilde{\nu}_{CO_2}CO_2(g) + \tilde{\nu}_{CH_4}CH_4(g) + \tilde{\nu}_{H_2}H_2(g) + \tilde{\nu}_{tar_{inert}}tar_{inert} \quad (17)$$

The stoichiometric coefficients $\tilde{\nu}_j$ of each species are reported in Table 2. For the reaction rate $\dot{r}_{j,crack}$ (kg/kg/s), the kinetic model by Boroson and Howard (1989) is used

$$\dot{r}_{j,crack} = \tilde{\nu}_j \cdot 10^{4.98} \cdot \exp^{(-93.37/RT_{par})} \cdot (w_{g,tar}\,\rho_g) \quad (18)$$

where $(w_{g,tar}\,\rho_g)$ is the amount of tar in the gas phase. According to the experimental investigation by Rath and Staudinger (2001), only 78% of the initial tar is cracked and 22% remains unchanged (see Table 2).

Homogeneous gas-phase reactions

Reactive gas species are produced during drying and pyrolysis of biomass and react with each other (such as water gas shift reaction) or with primary-air oxygen. The heat generated by exothermic reactions is important for the release of pyrolysis gases, formation of soot, or ignition of char. In the present work the following four homogeneous reactions are considered

$$CO + H_2O \xleftrightarrow{k_1} CO_2 + H_2 \quad (19)$$

$$2CO + O_2 \xrightarrow{k_2} 2CO_2 \quad (20)$$

$$2H_2 + O_2 \xrightarrow{k_3} 2H_2O \quad (21)$$

$$CH_4 + 2O_2 \xrightarrow{k_4} CO_2 + 2H_2O \quad (22)$$

Reaction 19 is an equilibrium limited reaction (Table 3). At lower temperatures, it favors the production of CO_2 and H_2, and at higher temperatures CO and H_2O. The equilibrium constant K is computed from the free Gibbs enthalpies of the reaction. The equilibrium of reactions 20–22 is far on the product side and, therefore, reverse reactions can be neglected. All kinetic parameters are taken from literature as given in Table 3.

Heterogeneous reactions

Heterogeneous reactions are those of char (that is, the solid pyrolysis residue) with species in the gas phase (such as O_2, CO_2, H_2O). These complex reactions were investigated by Fredersdorff and Elliott (1963), who assumed that O_2 dissociatively chemisorbs at free active sites of the carbon lattice and creates a C(O) complex and free oxygen radicals O as intermediate products. In a next reaction step, this C(O) complex forms free CO and CO_2. The mechanism of char-CO_2 and H_2O reactions is similar to the char-O_2 reaction (Laurendeau, 1978). This work uses a simplified reaction model that considers the following overall reactions

$$2\frac{\eta+1}{\eta+2}C + O_2 \xrightarrow{k_5} \frac{2\eta}{\eta+2}CO + \frac{2}{\eta+2}CO_2 \quad (23)$$

$$C + CO_2 \xrightarrow{k_6} 2CO \quad (24)$$

$$2C + H_2O \xrightarrow{k_7} CO + H_2 \quad (25)$$

The ratio η of CO to CO_2 production changes with temperature, as given in Table 4. The rate expressions and kinetic parameters are summarized in Table 4. In this table $(1-X_C)^{1.2}$ is the amount of unreacted carbon, and the empirical exponent 1.2 takes into account the change of the available reactive surface during the reactions (Dutta et al., 1977; Di Blasi et al., 1999).

Table 3. Rate Expressions for Homogeneous Gas-Phase Reactions (mol/m³/s)

de Souza-Santos (1989)

$$\dot{r}_1 = 2.78\times10^{-3}\cdot\exp\left(\frac{-1{,}510}{T_g}\right)\cdot\left(y_{CO}\,y_{H_2O} - \frac{y_{CO_2}\,y_{H_2}}{K}\right)\cdot c_{mol}^2$$

Groppi et al. (2000)

$$\dot{r}_2 = 3.98\times10^{14}\cdot\exp\left(\frac{-20{,}119}{T_g}\right)\cdot y_{CO}\,y_{O_2}^{0.25}\,y_{H_2O}^{0.5}\cdot c_{mol}^{1.75}$$

Groppi et al. (2000)

$$\dot{r}_3 = 2.19\times10^{12}\cdot\exp\left(\frac{-13{,}127}{T_g}\right)\cdot y_{H_2}\,y_{O_2}\cdot c_{mol}^2$$

Groppi et al. (2000)

$$\dot{r}_4 = 1.58\times10^{13}\cdot\exp\left(\frac{-24{,}343}{T_g}\right)\cdot y_{CH_4}^{0.7}\,y_{O_2}^{0.8}\cdot c_{mol}^{1.5}$$

Physical properties

Several physical data such as fuel density, thermodynamic, and transport properties are required for the simulation of a biomass fuel bed. All properties are calculated depending on temperature, pressure, and degree of conversion according to literature (see references in Table 5).

The density of the gas phase is given by the ideal-gas law, and the density of the moisture is calculated as a function of its temperature. Depending on the degree of devolatilization, the density of the solid phase changes from one of wood to the density of char including ash. The enthalpy and heat capacity of the gas phase depend on temperature and gas composition. The heat capacity of the particles is an average of

Table 4. Rate Expressions for Heterogeneous Combustion and Gasification Reactions

Di Blasi et al. (1999)	
$\dot{r}_5 = 1.5\times10^6 \cdot \exp\left(\frac{-13{,}078}{T_{\text{par}}}\right) \cdot p_{O_2} \cdot (1-X_C)^{1.2}$	(1/s)
Monson et al. (1995)	
$\eta = 3\times10^8 \cdot \exp\left(\frac{-30{,}178}{T_{\text{par}}}\right)$	
Biggs and Agarwal (1997)	
$\dot{r}_6 = 4{,}364\times\exp\left(\frac{-29{,}844}{T_{\text{par}}}\right) \cdot c_{CO_2}$	(mol/m^2/s)
Mühlen et al. (1985)	
$\dot{r}_7 = \frac{k_7 \cdot p_{H_2O}}{1 + k_8 \cdot p_{H_2O} + k_9 \cdot p_{H_2}}$	(1/s)
$k_7 = 4.93\times10^3 \cdot \exp\left(\frac{-18{,}522}{T_{\text{par}}}\right)$	(1/bar/s)
$k_8 = 1.11\times10^1 \cdot \exp\left(\frac{-3{,}548}{T_{\text{par}}}\right)$	(1/bar)
$k_9 = 1.53\times10^{-9} \cdot \exp\left(\frac{+25{,}161}{T_{\text{par}}}\right)$	(1/bar)

wood, moisture, and ash, and changes according to the particle consumption.

The transport properties in the model comprise the Ergun and Darcy parameters, diffusion, conduction, and heat-/mass-transfer coefficients. The Ergun parameters are given as a function of the particle geometry, gas viscosity, and bed porosity. The permability of the individual particles increase linearly with the degree of devolatilization. The diffusion coefficients are based on binary diffusion coefficients that are adapted by the simplifying Wilke-equation for a multicomponent gas mixture. Within the packed bed, an effective diffusion coefficient is applied that incorporates also dispersive transport effects. This dispersion is due to turbulence and back-mixing, and depends on the flow velocity, particle size, and bed porosity. Within the particles, an effective particle diffusion coefficient is used where the particle tortuosity and porosity are taken into account. The heat conductivity of the wood particles is calculated as a function of the particle porosity, moisture content and by an arithmetic mean of the wood heat conductivity, transverse and longitudinal to the fiber direction. This seems to be reasonable, because the individual particles in the bed are arranged anisotropically, and because in a 1-D particle-model only one mean particle direction can be considered. The effective thermal conductivity of the bed is evaluated as a function of the bed porosity, particle size, and temperature. In this approach the effects of gas conduction, solid conduction, gas-solid heat transfer, and radiative heat transport are lumped together. The heat and mass transfer between the single particles and the gas phase of the bed are computed using Nusselt and Sherwood correlations for fixed beds. For the single particle simulations, transfer coefficients for single spheres are applied.

In the presented work the simplifying assumption of spherical particles is chosen, but other particle geometries can also be modeled with the 1-D + 1-D-concept. The single particle model can be applied, for example, in cylindrical coordinates and the approaches for the transport properties within the bed can be extended by using shape factors.

Particle and bed shrinkage

During the thermal conversion of biomass, the size of the individual particles changes. The size of beech wood particles is reduced by 10% (Simpson and Ten Wolde, 1999) due to drying. Experimental investigations of the pyrolysis of beech wood (Hochegger, 2000) show that the particle size also shrinks by 10%. Thus, in the present model, it is assumed that during drying and pyrolysis the particle diameter remains constant and only its porosity changes (Di Blasi, 2000). Contrary to drying and pyrolysis, the decrease in the particle size cannot be neglected during char combustion and is considered in our model. As shown in Figure 2, a 1-D + 1-D grid is set up for the single particles within the packed bed. This spatial grid remains unchanged during the simulations, that is, if outer layers of the solid particle structure are totally consumed, particle gridpoints with a porosity of 100% are obtained. This is taken into account within the model of the single particles and also within the model of the entire bed. Therefore, our model accounts for particle and bed shrinkage during biomass conversion.

Table 5. Physical Properties of the Fuel Bed

Density of moisture	ρ_l	Verein Deutscher Ingenieure (1991)
Density of solid	ρ_s	Simpson and Ten Wolde (1999)
Heat capacity, enthalpy of gas	$c_{p,g}$, h_g	Barin (1985)
Heat capacity of moisture	$c_{p,l}$	Verein Deutscher Ingenieure (1991)
Heat capacity of dry wood	$c_{p,s}$	Richardson (1993)
Ergun parameters	A_E B_E	Verein Deutscher Ingenieure (1991)
Permeability	C_D	Siau (1984)
Binary diffusion coefficient	$D_{i,j,\text{bin}}$	Fuller et al. (1966)
Diffusion coefficient in mixture	$D_{i,j}$	Taylor and Krishna (1993)
Effect. diffusion coeff. of bed	$D_{\text{eff,bed}}$	Tsotsas and Schlünder (1988)
Effect. diffusion coeff. of particle	$D_{\text{eff,par}}$	Szekely et al. (1976)
Heat conductivity of gas	λ_g	Verein Deitscher Ingenieure (1991)
Heat conductivity of moisture	λ_l	Verein Deutscher Ingenieure (1991)
Heat conductivity of bed	$\lambda_{\text{eff,bed}}$	Vortmeyer (1980)
Heat conductivity of particle	$\lambda_{\text{eff,par}}$	Siau (1984)
Mass/heat transfer in bed	α_{bed}, β_{bed}	Winterberg et al. (1999)
Mass/heat transfer, single particle	α_{par}, β_{par}	Verein Deitscher Ingenieure (1991)

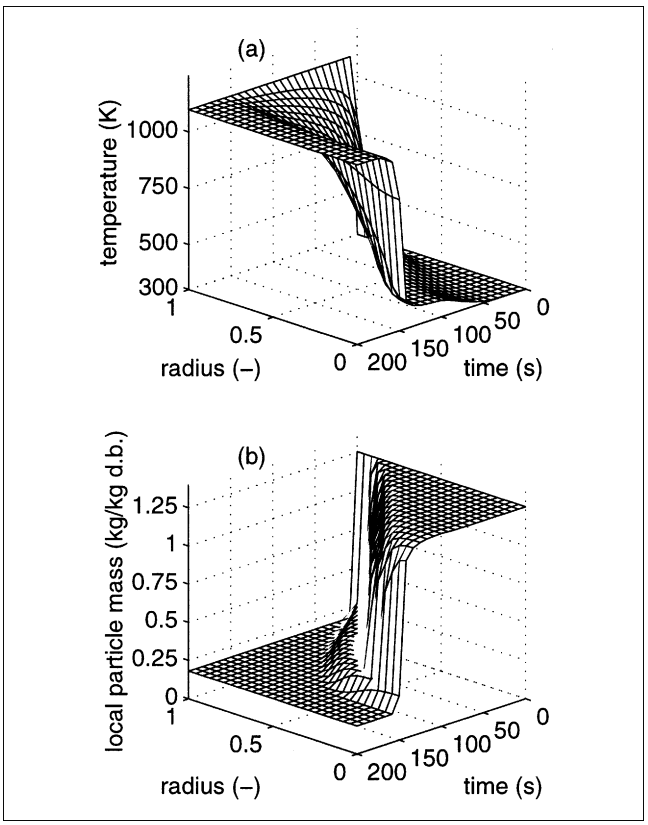

Figure 4. Temperature and local relative particle mass during drying and pyrolysis of a single beech particle.

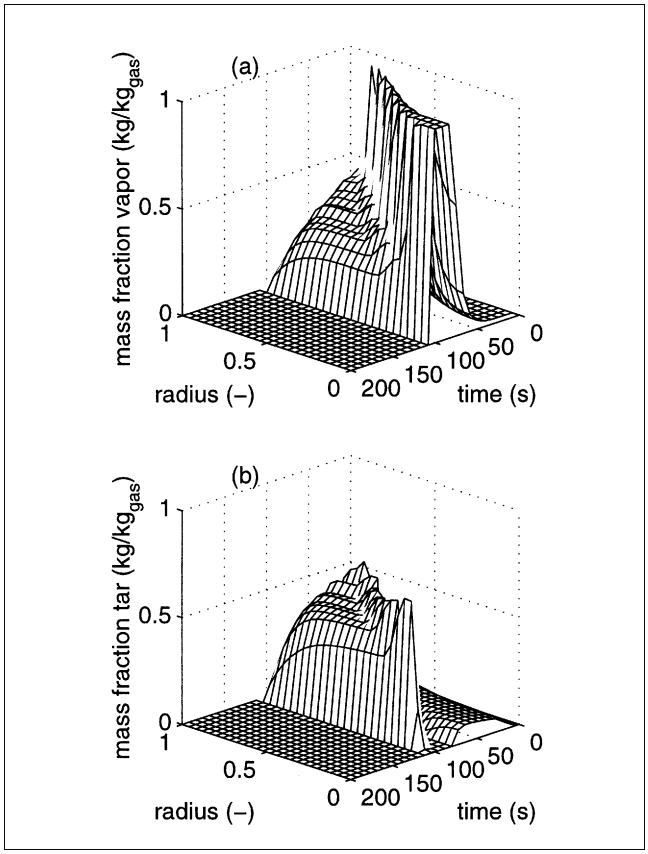

Figure 5. H_2O and tar mass fraction during drying and pyrolysis of a single beech particle.

Results

In this section, validation simulations for single particles are presented, followed by the results obtained by using the 1-D + 1-D model of biomass combustion on a moving grate.

Validation

Validation simulations for single particles (spherical 20 mm beech particle with 25% moisture exposed to a N_2 atmosphere) were performed for conditions corresponding to experimental investigations (Petek, 1998; Hochegger, 2000). Figure 4 shows particle temperature and solid mass, and Figure 5 presents H_2O-vapor, and tar mass fractions during drying and pyrolysis. The temperature of the particle (Figure 4a) is shown as a function of the particle radius and the reaction time. Initially, the particle temperature is 298 K, and the surrounding temperature is maintained at 1,098 K. First, the temperature increases at the particle surface and remains constant (wet bulb temperature) for a short period of time due to drying. This effect becomes more pronounced as the drying front moves into the particle, since drying is controlled by intra-particle heat transfer. At the particle center, the wet bulb temperature is sustained from 60 s to 140 s. As soon as the particle is dry, the temperature rises quickly until the entire particle reaches the temperature of the surrounding gas. Similar to the temperature profile, the plot of the local relative particle mass (Figure 4b) shows several distinctive features. At the beginning, the entire solid and moisture mass is 125% of the dry particle. The steep decrease of the local relative mass is mainly caused by pyrolysis of tar, which is the largest part of the volatiles. The plateau at about 0.28 kg/kg d.b. represents the amount CO and CO_2 of the pyrolysis gases. Compared to tar, these gases are produced at higher temperatures with a lower reaction rate. Once CO and CO_2 are volatilized, the relative mass of the particle decreases to 0.18 kg/kg d.b.—the mass of the remaining char. The mass fraction of H_2O in the gas phase (Figure 5a) remains low in the beginning, and, at the particle center, no vapor is present for the first 35 s. During this period, pyrolysis of tar already occurs at the particle boundary, where the temperatures are high enough for this reaction. Both tar and vapor are transported towards the center of the particle, where the temperature is still low and where the gas-phase vapor condenses. Tar remains as the main gas component and, therefore, the tar mass fraction (Figure 5b) shows a small peak at the particle center at 30 s. Tar condensation is not taken into account due to its small impact on the process (Di Blasi, 1996). Subsequently, the tar fraction decreases to 8%, whereas H_2O shows a distinctive peak due to drying. Once the whole particle is dry, the fraction of H_2O decreases continuously, since it is replaced by pyrolysis products. The tar fraction increases briefly after drying and goes to zero when pyrolysis is completed. At this time, the entire pore system is filled with N_2 from the surrounding gas.

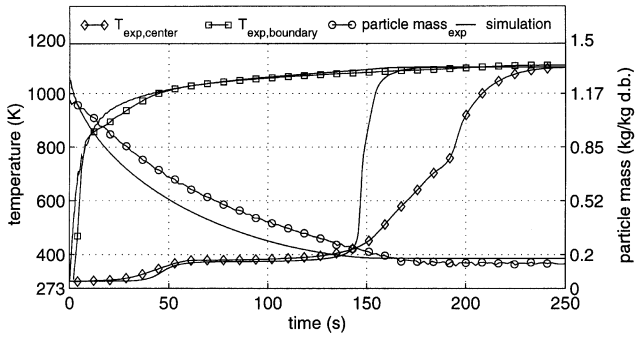

Figure 6. Mass conversion (○), particle center (◇) and surface (□) temperature during drying and pyrolysis of a 20 mm beech particle with a moisture content of 25% d.b., and constant ambient temperature of 1,098 K.

A comparison of these simulation results with experimental data is shown in Figure 6. Experimental data were obtained in a thermo-balance designed for large particles (Rath et al., 2002). In the experiment, a particle is released into a preheated oven that is flushed with N_2 at a given temperature. Particle surface, center temperature and mass loss are measured as a function of the reaction time. Experimental and simulated particle surface temperature shows a good agreement as seen in Figure 6. Thus, the model for the heat transfer between the particle surface and the gas bulk in the thermo-balance oven seems to be reasonable. In Figure 6 both experimental and simulation results show a distinct temperature difference between particle surface and center due to intraparticle heat transfer. This fact confirms the need for a comprehensive single particle model for high heating rates, since the assumption of isothermal particles is clearly not justified under those conditions. Until 140 s, the particle center temperature is more or less constant at the wet bulb temperature, and, as soon as the particle is dry, the temperature rises. However, the simulated temperature deviates from the experimental results because of changing char properties such as density, heat capacity, and heat conductivity. In order to improve the simulations, a new and more accurate model for the char properties is under development. The particle mass continuously decreases from 125% to about 18% of the initial dry mass within 170 s, and it can be seen that simulation and experimental data agree very well.

Figure 7a shows the total mass loss of a single 20 mm particle with 8% moisture exposed to different atmospheres. In the simulations, the temperature of the ambient atmosphere is kept constant at 1,223 K, according to experimental conditions (Petek, 1998). In a N_2 atmosphere only drying and pyrolysis occurs, and, after about 100 s, the particle reaches 18% of the initial mass corresponding to the remaining char. In CO_2, however, the char is gasified and totally consumed after approximately 950 s. Conversion in an O_2 atmosphere of air is the fastest process and the particle is consumed after about 180 s. The mass curves of the 20 mm particle coincide up to 80 s, where char reactions are not dominant. This can be explained by two facts. First, ignition of heterogeneous reactions occurs at temperatures that are higher than the ones during pyrolysis. Second, char reactions are controlled by the

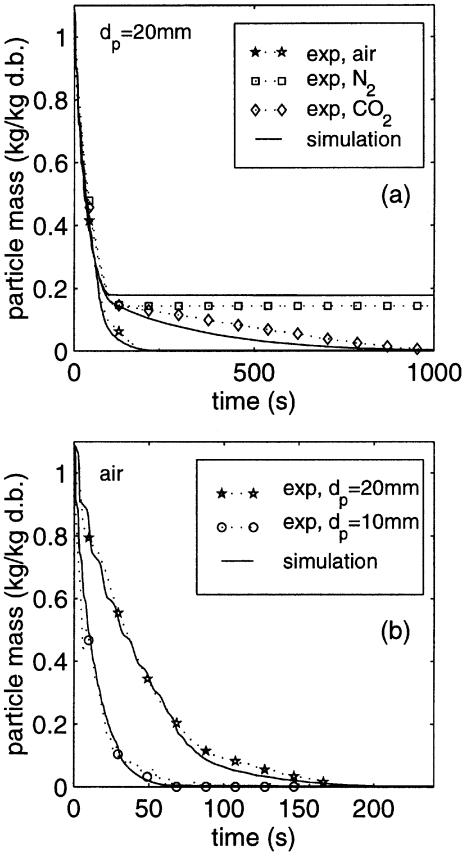

Figure 7. Mass loss of a 20 mm beech particle with 8% moisture in air, N_2, CO_2 (a), and particles of different diameter in O_2 (b).

Ambient temperature is 1,223 K.

transport of reactive species from the surrounding gas phase. As long as gaseous species are released due to pyrolysis, convective mass transport of the volatiles prevents CO_2 or O_2 from diffusing into the particle. Once O_2 penetrates the outer layers, the particle ignites, and the subsequent temperature rise accelerates pyrolysis in the final stage. Conversion of particles with different diameters in an O_2 atmosphere is shown in Figure 7b. It can be seen that a reduction of the diameter by the factor two reduces the total conversion time by 65%.

In Figure 8 and Figure 9 the particle temperatures corresponding to the four cases in Figure 7 (air, N_2, CO_2, $d_p = 10$ mm, $d_p = 20$ mm) are shown. The temperature profile that develops in a N_2 atmosphere (Figure 8a) is similar to that in Figure 4. However, the time range has changed due to lower moisture content and a higher ambient temperature. The particle heats up, sustains the wet bulb temperature for a short period of time, and heats up again to reach the ambient temperature. The profile calculated for the gasification in a CO_2 atmosphere (Figure 8b) is initially similar to the one in N_2, since drying and pyrolysis are the dominating effects. Once these stages are completed, endothermic gasification starts, which causes a temperature difference between the surface and the particle center of about 80 K. This profile is a pseudo-steady state, which is determined by the heat trans-

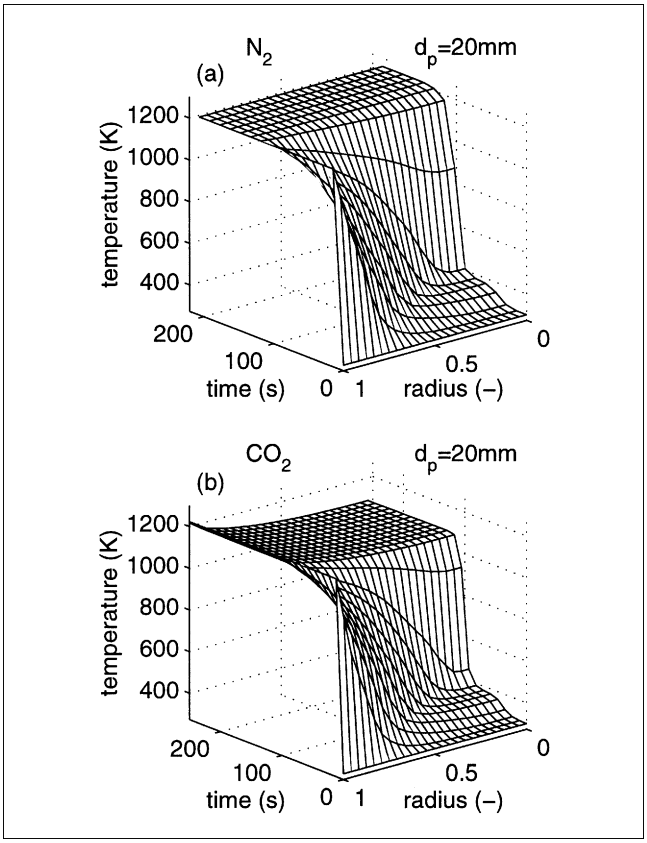

Figure 8. Temperature of 20 mm particles as a function of radius and time for drying, pyrolysis, and char conversion in different atmospheres (N_2, CO_2).

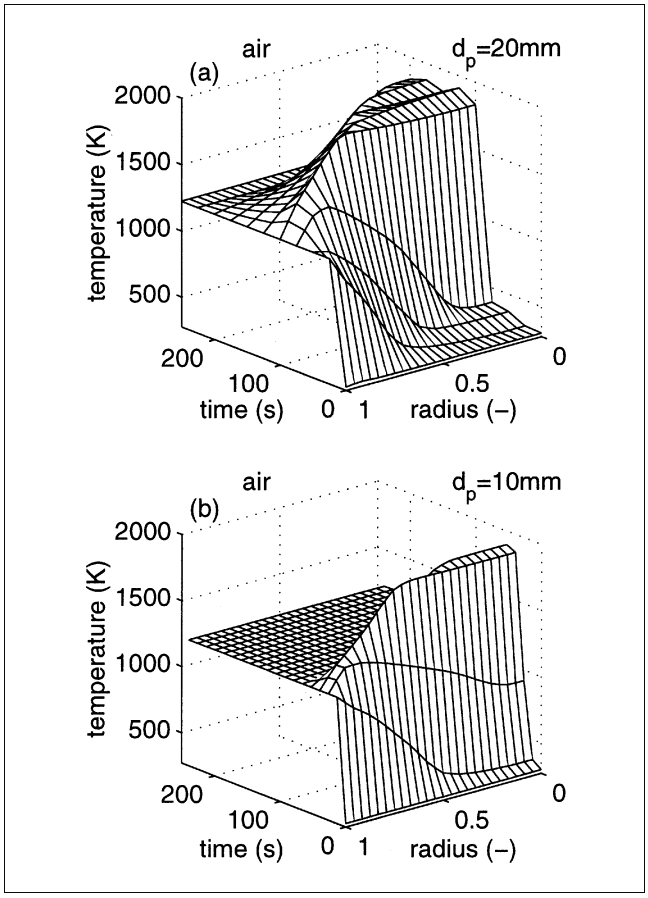

Figure 9. Particle temperature as a function of radius and time for drying, pyrolysis, and char conversion in air for different particle diameters (10 mm, 20 mm).

port in the particle and the endothermic gasification reaction. As soon as the char is completely converted, the temperature rises to the ambient level. The temperature profiles for conversion in air (Figures 9a and 9b) have a significantly different shape. The particle undergoes drying and pyrolysis until the combustion reactions start, leading to a temperature maximum at the particle center, where no cooling by the surrounding gas occurs. For smaller particles (Figure 9b), pyrolysis and combustion are accelerated because of the reduced intraparticle mass and heat transfer. The region of high temperature occurs at a particle radius smaller than the initial radius and moves to the particle center. This is due to the fact that the outer solid layers are completely consumed, causing particle shrinkage.

Combustion of biomass

In our simulations of the thermal biomass conversion on a moving grate typical operating conditions were chosen. The bed has a height of 30 cm and consists of 30 mm beech particles with a moisture content of 30% d.b. The bed is supplied with primary air from the grate with a temperature of 298 K and a superficial velocity of 0.1 m/s. The bed is ignited at its surface by radiation from the combustion chamber. The bed surface temperature is assumed to be 1,173 K and constant over the length of the grate. This may be an approximation, but a detailed description of the surface temperature would require a combined packed bed and furnace chamber model.

Figures 10–13 show the temperature, the mass fractions of H_2O (vapor), and tar in the gas phase (kg_j/kg_{gas}), and the entire bed conversion at different reaction times (600 s and 1,700 s), representing different positions along the moving grate (see previous section). Each variable is given as a function of bed height and particle radius. The profiles within individual particles are shown as a function of the radial coordinate and the height of the bed. Figure 10 and Figure 11 show the early stage of biomass conversion (600 s). Three quarters of the bed remain at initial and primary air temperature, and only the topmost layer reaches the bed surface temperature (Figure 10a). In this region, there is a temperature gradient in the radial direction with lower temperatures at the particle surface and higher temperatures within the particle that are caused by exothermic char reactions. Due to the endothermic drying process, there is a small area of constant 373 K at 62% bed height near the particle center. Drying and pyrolysis occur at different temperatures and, therefore, they are located at different bed heights, which can be seen in the plots of the H_2O and tar gas-phase mass fractions (Figures 11a and 11b). The H_2O fraction shows a peak at 62% bed

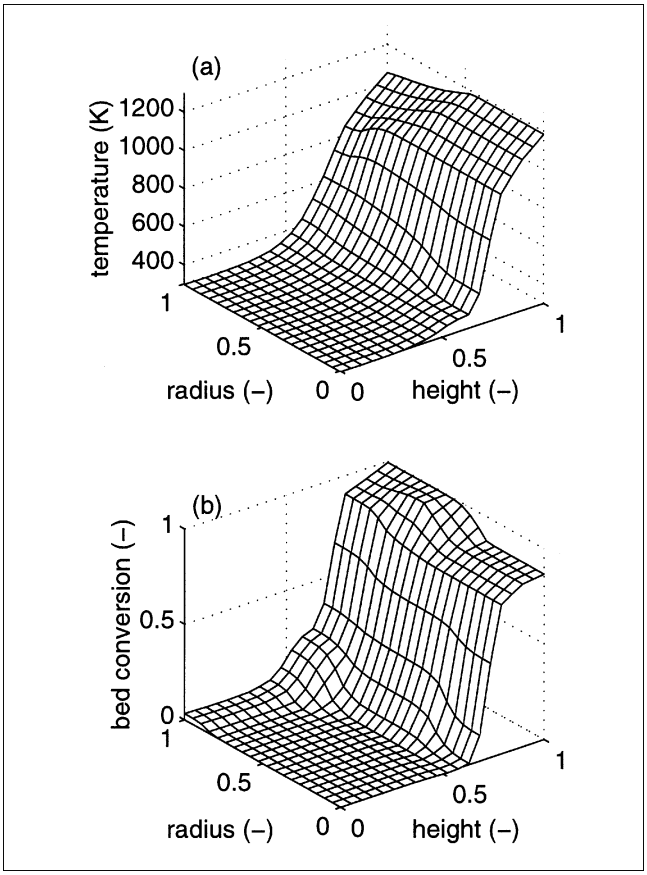

Figure 10. Temperature and bed conversion at 600 s.

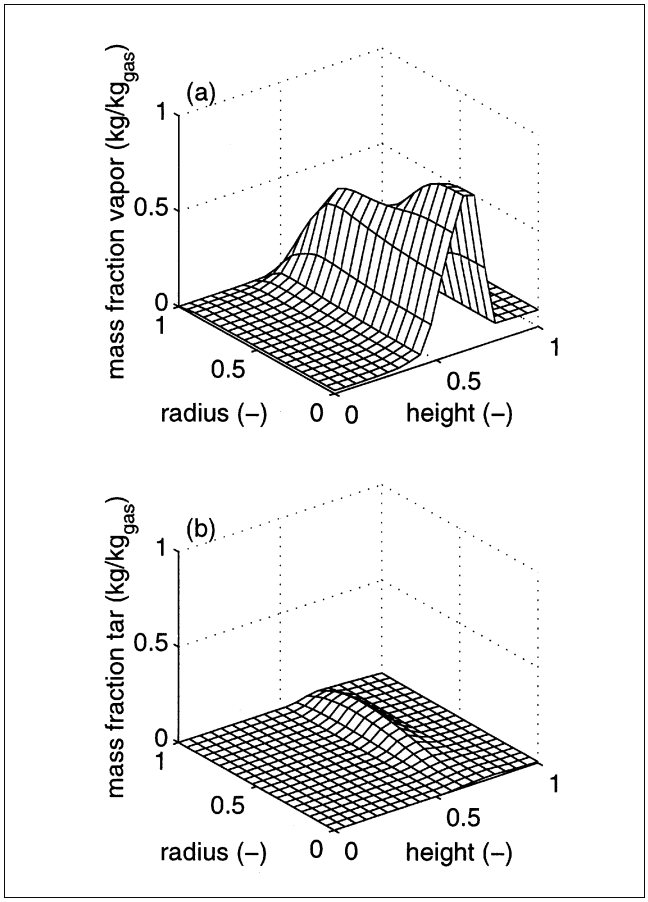

Figure 11. H_2O and tar mass fraction at 600 s.

height, corresponding to the position of the drying front. Below that, temperatures are too low for drying, and, above that, drying is finished and vapor is replaced by pyrolysis gases. The tar peak, for example, follows directly the drying front and shows a decline near the particle center where drying still takes place. In the plot of the bed conversion (Figure 10b), the effects of drying, pyrolysis and char combustion can be distinguished. In the lower half of the bed, no conversion has occurred yet. In the upper half, initial bed conversion is due to drying, followed by pyrolysis which results in approximately 87% conversion. The conversion from 87% to 100% is due to char reactions that are completed only at the outer half of the topmost particles.

Figures 12 and 13 show the same systems as Figure 10 and Figure 11 at 1,700 s. The region of high temperatures has moved from the top of the bed, and is located closer to the grate (Figure 12a). At this point, the char combustion causes a local maximum of about 1,245 K, and decreases in the direction of the particle surface, which is caused by the cool primary air. Above that, the temperature finally reaches the value of the boundary condition. Particles no longer exist above the char reaction front, which is indicated by an absence of intraparticle gradients and only a small gradient in the direction of the bed height. Within this region, the particle and bed heat conductivity was equal to the bulk properties in order to describe the effect of a shrinking bed. The H_2O mass fraction (Figure 13a) shows a peak at 30% bed height. Above that, the system is dry and vapor is replaced by other gases, as indicated by the tar peak (Figure 13b). This peak coincides with a steep decrease of the bed conversion (Figure 12b). The conversion between 87% and 100% occurs at the same position as the temperature peak due to char combustion. Above that, one-third of the entire bed is completely consumed.

Figures 10–13 show the transient behavior of the thermal bed conversion with the exothermic conversion front moving towards the bottom part of the grate area. The front moving velocity, which is influenced by fuel and operation conditions, is constant over a major part of the entire bed conversion. This is shown in Figure 14, where the bed mass is plotted as a function of reaction time and bed height. The bed conversion slows down only when the particle layer at the grate surface starts being consumed because of primary air cooling (298 K). Over the entire bed height (0.0 m and 0.3 m), the curves of the relative mass show a similar shape. Drying takes place between 1.3 kg/kg d.b. and 1.0 kg/kg d.b., and is followed by pyrolysis of tar and H_2O that reduce the solid mass to 0.30 kg/kg d.b. After CO and CO_2 are volatilized, the mass is reduced from 0.18 kg/kg d.b. to zero due to char combustion. After approximately 3,200 s, the bed is completely consumed and only a small amount of ash (1%) remains. The result of the total burnout time, combined with the horizontal bed migration velocity, can be used to determine the required grate length of biomass furnaces.

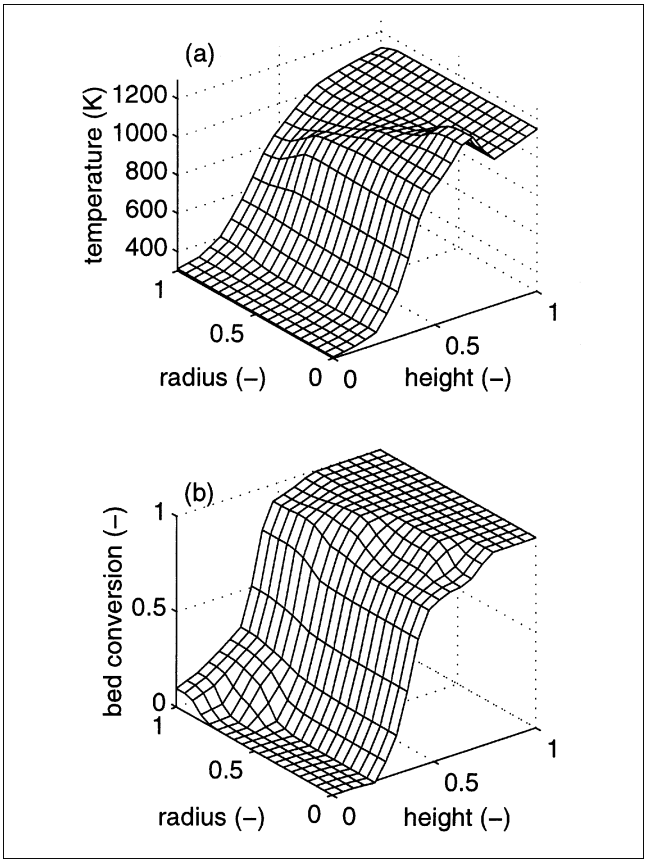

Figure 12. Temperature and bed conversion at 1,700 s.

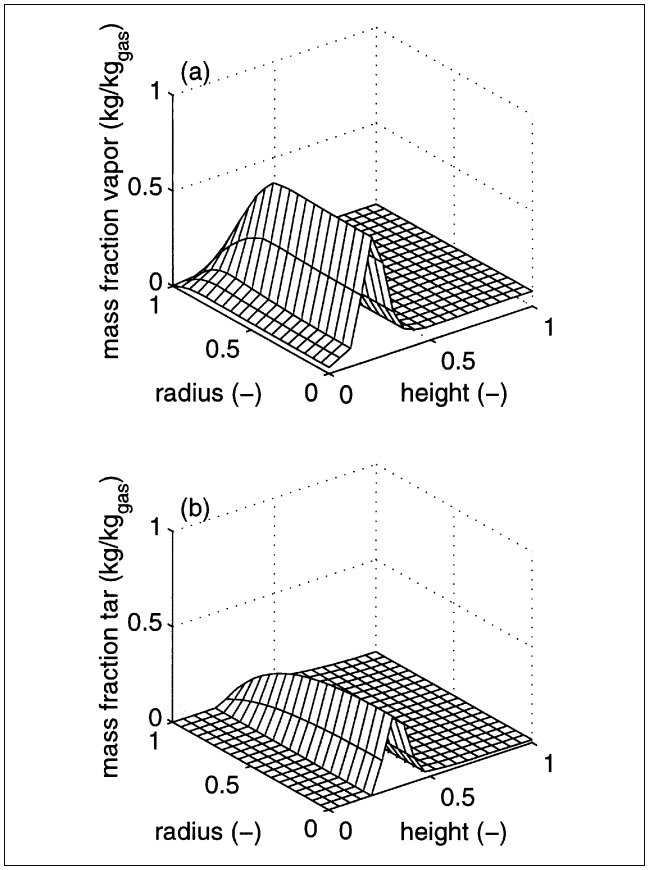

Figure 13. H_2O, tar mass fraction at 1,700 s.

Conclusions

A comprehensive model of packed biofuel beds consisting of single porous particles is presented and kinetic data for drying, primary and secondary pyrolysis, gasification, and combustion are summarized. The single particle model is validated by comparing experimental and numerical results, which show good agreement for drying, pyrolysis, gasification in CO_2 and combustion in air atmosphere. It can be concluded that the single particle model—a cornerstone of packed-bed models of large particles and high volatile fuels —generates reliable results. Also, simulation results for an entire biomass bed are presented. The simulation results show that traveling drying, pyrolysis, and char conversion fronts exist in the reactor at different positions. Thus, the different conversion mechanisms do not occur simultaneously at a given bed height. An important result of the simulations is the time needed for the complete burnout of the bed. This time strongly depends on the fuel conditions (such as kind of wood and moisture content) and operation conditions such as the primary air flow rate and temperature, bed height, and the temperature of the combustion chamber. The total burnout time is a decisive information for the design of grate furnaces, since it is needed for the estimation of the grate length and the size of the entire furnace. Thus, the presented model can be used to perform investigations of different furnace conditions and may be used for the optimization of existing furnaces and the development of new ones.

Future work will address the influence of the bed surface temperature on bed ignition behavior and on conversion front velocities. Particular attention will be paid to the coupling of the bed model with a furnace chamber model, such that simulations of an entire biomass boilers can be performed.

Acknowledgments

This work was funded in part by the European Commission in the framework of the nonnuclear energy program, Joule III, in contract JOR3-CT980278.

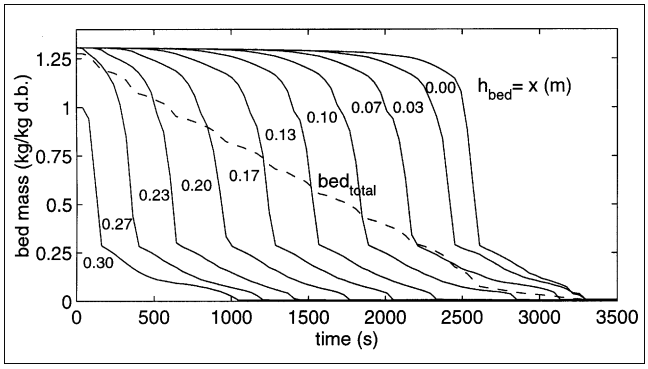

Figure 14. Bed mass during thermal conversion at different bed heights.

Notation

a = specific surface, m^2/m^3
A = Ergun coefficient, $Pa \cdot s/m^2$
B = Ergun coefficient, $Pa \cdot s^2/m^3$
c = molar concentration, mol/m^3
c_p = heat capacity, J/kg/K
C = permeability, $1/m^2$
D = diffusion coefficient, m^2/s
E = activation energy, kJ/mol
h = enthalpy, J/kg
Δh = reaction enthalpy, J/mol
K = equilibrium constant, variable
k = reaction constant, variable
k_0 = frequence factor, variable
MG = molar mass, kg/mol
$\dot{m}$ = mass flux, $kg/m^2/s$
p = pressure, Pa
p^* = equilibrium pressure, Pa
r = coordinate in a spherical system, m
$\dot{r}$ = reaction rate, variable
R = gas constant, J/mol/K
R = particle radius, m
R = number of reactions
S = number of species
T = temperature, K
t = time, s
v = gas velocity, m/s
w = mass fraction
X = conversion rate
y = mol fraction
z = coordinate in a Carthesian system, m

Greek letters

α = heat-transfer coefficient, $W/m^2/K$
β = mass-transfer coefficient, $kg/m^2/s$
Γ = general diffusion coefficient, variable
ϵ = volume fraction
η = fraction of CO to CO_2
η = viscosity, Pas
κ = general transfer coefficient, variable
λ = heat conductivity, W/m/K
ν = stoichiometric coefficient
$\tilde{\nu}$ = mass specific coefficient
ρ = density, kg/m^3
Φ = general variable, variable
φ = correction function

Superscripts and subscripts

bed = packed bed
C = char
crack = cracking
D = Darcy
dry = drying
E = Ergun
eff = effective
FSP = fiber saturation point
g = gas phase
het = heterogeneous
hom = homogeneous
i = reaction index
j = species index
l = liquid phase
mol = molar
par = particle
pyro = pyrolysis
S = saturation
s = solid phase

Literature Cited

Alves, S. S., and J. L. Figueiredo, "A Model for Pyrolysis of Wet Wood," *Chem. Eng. Sci.*, **44**, 2861 (1989).

American Bioenergy Association, "Biomass: Clean Energy for America's Future," available on the web at http://www.biomass.org/fact_sheet_2.htm (2000).

Amundson, N. R., and L. E. Arri, "Char Gasification in a Countercurrent Reactor," *AIChE J.*, **24**, 87 (1978).

Antal, M. J. J., H. L. Friedman, and F. E. Rogers, "Kinetics of Cellulose Pyrolysis in Nitrogen and Steam," *Combustion Sci. and Technol.*, **21**, 141 (1980).

Barin, I., *Thermochemical Data of Pure Substances*, Vol. 1, 3rd ed., Wiley, New York, London, and Sydney (1985).

Beenackers, A. A. C. M., "Biomass Gasification in Moving Beds, a Review of European Technologies," *Renewable Energy*, **16**, 1180 (1999).

Biggs, M. J., and P. K. Agarwal, "The CO/CO_2 Product Ratio for a Porous Char Particle Within an Incipiently Fluidized Bed: A Numerical Study," *Chem. Eng. Sci.*, **52**, 941 (1997).

Bliek, A., W. M. van Poelje, W. P. M. van Swaaij, and F. P. H. van Beckum, "Effects of Intraparticle Heat and Mass Transfer During Devolatilization of a Single Particle," *AIChE J.*, **31**, 1666 (1966).

Boroson, M. L., and J. Howard, "Product Yields and Kinetics from Vapor Phase Cracking of Wood Pyrolysis Tars," *AIChE J.*, **35**, 120 (1989).

Bridgwater, A. V., "The Technical and Economical Feasibility of Biomass Gasification for Power Generation," *Fuel*, **74**, 634 (1995).

Bryden, K. M., and W. Ragland, "Numerical Modeling of a Deep Fixed Bed Combustor," *Energy & Fuel*, **10**, 269 (1995).

Cenkowski, S., D. S. Jayas, and S. Pabis, "Deep-Bed Grain Drying—A Review of Particular Theories," *Drying Technology*, **11**, 1553 (1993).

Chejne, F., J. P. Hernandez, W. F. Florez, and A. F. J. Hill, "Modelling and Simulation of Time Dependent Coal Combustion Process in Stacks," *Fuel*, **79**, 987 (2000).

Cooper, J., and W. L. Hallet, "A Numerical Model for Packed-Bed Combustion of Char," *Chem. Eng. Sci.*, **55**, 4451 (2000).

de Souza-Santos, M. L., "Comprehensive Modelling and Simulation of Fluidized Bed Boilers and Gasifiers," *Fuel*, **68**, 1507 (1989).

Deuflhard, P., E. Hairer, and J. Zugck, "One Step Extrapolations Methods for Differential-Algebraic Systems," *Numerical Mathematics*, **51**, 501 (1987).

Di Blasi, C., "Modeling and Simulation of Combustion Processes of Charring and Non-Charring Solid Fuels," *Chem. Eng. Sci.*, **19**, 71 (1993).

Di Blasi, C., "Heat Momentum and Mass Transport through a Shrinking Biomass Particle Exposed to Thermal Radiation," *Chem. Eng. Sci.*, **51**, 1121 (1996).

Di Blasi, C., "Dynamic Behaviour of Stratified Downdraft Gasifiers," *Chem. Eng. Sci.*, **55**, 2931 (2000).

Di Blasi, C., F. Buonanno, and C. Branca, "Reactivities of some Biomass Chars in Air," *Carbon*, **37**, 1227 (1999).

Dieterich, E. E., "Systematische Bilanzierung und modulare Simulation verfahrenstechnischer Apparate," Diss. Univ. Stuttgart, Wissenschaftsverlag Aachen (1998).

Dry, R. J., and R. D. La Nauze, "Combustion in Fluidized Beds," *Chem. Eng. Process*, **86**(7), 31 (1980).

Dutta, S., C. Y. Wen, and R. J. Belt, "Reactivity of Coal and Char: 2. In Oxygen Nitrogen Atmosphere," *Ind. Eng. Chem. Process Des. and Dev.*, **16**, 31 (1977).

Eigenberger, G., "On the Dynamic Behavior of the Catalytic Fixed Bed Reactor in the Region of Multiple Steady States: 1. The Influence of the Heat Conduction in Two Phase Models," *Chem. Eng. Sci.*, **27**, 1909 (1972).

Ergun, S., "Fluid Flow through Packed Columns," *Chem. Eng. Sci.*, **48**(2), 89 (1952).

European Commission, "Energy for the Future: Renewable Sources of Energy," White Paper for a Community Strategy and Action Plan, European Commission, Brussels, available on the Web at http://europa.eu.int/comm/energy/en/ctore.htm (1997).

EuroREX: The European Union, General Information available on the Web at http://www.eurorex.com/viewcountry.asp?viewL3 = N &country%ID = 31 (2000).

Fredersdorff, C. G., and M. A. Elliott, "Coal Gasification," *Chemistry of Coal Utilization*, H. H. Lowry, ed., Vol. 1 supplementary, Chapter 20, Wiley, New York, pp. 892–1022 (1963).

Fuller, E. N., P. D. Schettler, and J. C. Giddings, "A New Method for Prediction of Binary Gas-Phase Diffusion Coefficients," *Ind. and Chem. Eng.*, **58**(5), 18 (1966).

Govind, R., and J. Chah, "Modeling and Simulation of an Entrained Flow Coal Gasifier," *AIChE J.*, **30**, 79 (1984).
Groppi, G., E. Tronconi, P. Forzatti, and M. Berg, "Mathematical Modeling of Catalytic Combustors Fuelled by Gasified Biomasses," *Catalysis Today*, **59** (2000).
Hall, D., and J. House, "Biomass Energy Development and Carbon Dioxide Mitigation Options," *Int. Conf. on National Action to Mitigate Global Climate Change*, UNEP Collaborating Centre on Energy and Environment, Grafisk Service, Riso National Laboratory, Copenhagen, available on the web at http://www.uccee.org/CopenhagenConf/hall.htm (1995).
Hartner, P., "Entwicklung eines Computerprogramms zur Eindimensionalen Simulation von Heterogenen Festbett- und Vorschubreaktoren," PhD Thesis, Graz University of Technology (1996).
Hobbs, M. L., P. T. Radulovic, and L. D. Smoot, "Modeling Fixed-Bed Coal Gasifiers," *AIChE J.*, **38**, 681 (1992).
Hochegger, W., "Pyrolyse feuchter Biomass," Master Thesis, Graz University of Technology (2000).
Kalson, P. A., and D. E. Briggs, "Devolatilization and Tar Production in a Bituminous Lump Coal," *AIChE J.*, **31**, 1047 (1985).
Kaviany, M., *Principles of Heat Transfer in Porous Media*, Mechanical Engineering Series, Springer, Berlin (1991).
Laurendeau, N. M., "Heterogeneous Kinetics of Coal Char Gasification and Combustion," *Prog. in Energy Combustion Sci.*, **4**, 221 (1978).
Liliedahl, T., and K. Sjöström, "Modeling of Coal Pyrolysis Kinetics," *AIChE J.*, **40**, 1515 (1994).
Liu, S.-L., and N. R. Amundson, "Stability of Adiabatic Packed Bed Reactors. An Elementary Treatment," *I & EC Fundamentals*, **1**, 200 (1962).
Monson, C. R., G. J. Germane, A. U. Blackham, and L. D. Smoot, "Char Oxidation at Elevated Pressures," *Combust. and Flame*, **100**, 669 (1995).
Mühlen, H.-J., K. H. van Heek, and H. Jüngen, "Kinetic Studies of Steam Gasification of Char in the Presence of H_2, CO_2 and CO," *Fuel*, **64**, 944 (1985).
Neogi, D., C. C. Chang, W. P. Walawender, and L. T. Fan, "Study of Coal Gasification in an Experimental Fluidized Bed Reactor," *AIChE J.*, **32**, 17 (1986).
Petek, J., "Experimentelle Untersuchung der Pyrolyse in inerter und reaktiver Atmosphäre unter den Bedingungen der Wurfbeschickung," PhD Thesis, Graz University of Technology (1998).
Pitt, G. J., "The Kinetics of the Evolution of Volatile Products from Coal," *Fuel*, **41**, 267 (1962).
Rapagna, S., N. Jand, A. Kiennemann, and P. U. Foscolo, "Steam-Gasification of Biomass in a Fluidised-Bed of Olivine Particles," *Biomass and Bioenergy*, **19**, 187 (2000).
Rath, J., and G. Staudinger, "Cracking Reactions of Tar from Pyrolysis of Spruce Wood," *Fuel*, **80**, 1379 (2001).
Rath, J., G. Steiner, M. Wolfinger, and G. Staudinger, "Tar Cracking from Fast Pyrolysis of Large Beech Wood Particles," *J. of Analy. and Appl. Pyrolysis*, **62**, 83 (2002a).
Rath, J., M. Wolfinger, G. Krammer, F. Barontini, and V. Cozzani, "Heat of Pyrolysis," *Fuel*, in press (2002b).
Raupenstrauch, H., "Ein Beitrag zur Computersimulation reagierender Schüttschichten," PhD Thesis, Graz University of Technology (1991).
Richardson, M. J., "The Specific Heats of Coals, Cokes and their Ashes," *Fuel*, **72**, 1047 (1993).
Rummer, B., "Simulation der Trocknung, Pyrolyse und Vergasung großer Brennstoffpartikel," PhD Thesis, Graz University of Technology (1998).
Saastamoinen, J., Jaalkko, and R. K. Impola, "Drying of Solid Fuel Particles in Hot Gases," *Drying Technol.*, **13**, 1305 (1995).
Saastamoinen, J. J., R. Taipale, M. Horttanainen, and P. Sarkomaa, "Propagation of the Ignition Front in Beds of Wood Particles," *Combust. and Flame*, **123**, 214 (2000).
Schwleger, B., "Power from Wood," *Power*, **124**, 1 (1980).
Seebauer, V., "Experimentelle Untersuchungen zur Pyrolyse von Kohle und Holz," PhD Thesis, Graz University of Technology (1999).
Shin, D., and S. Choi, "The Combustion of Simulated Waste Particles in a Fixed Bed," *Combust. and Flame*, **121**, 167 (2000).
Siau, J. F., *Transport Processes in Wood*, Springer Series in Wood Science, Springer, Berlin (1984).
Simpson, W., and A. Ten Wolde, *Wood Handbook, Wood as an Engineering Material*, Tech. Rep. Physical Properties and Moisture Relation of Wood, U.S. Dept. of Agriculture, Madison, WI (1999).
Stillman, R., "Simulation of a Moving Bed Gasifier for a Western Coal," *IBM. J. Res. Dev.*, **23**, 240 (1979).
Szekely, J., J. W. Evans, and H. Y. Sohn, *Gas-Solid Reactions*, Academic Press, New York (1976).
Taylor, R., and R. Krishna, *Multicomponent Mass Transfer*, Wiley, New York (1993).
Thunmann, H., and B. Leckner, "Ignition and Progagation of a Reaction Front in Cross Current Bed Combustion of Wet Biofuel," *Fuel*, **80**, 473 (2000).
Tsotsas, E., and E. U. Schlünder, "On Axial Dispersion in Packed Beds with Fluid Flow," *Chem. Eng. Process*, **24**, 15 (1988).
Van den Broek, R., A. Faaij, and A. Van Wijk, "Biomass Combustion for Power Generation," *Biomass and Bioenergy*, **11**, 271 (1996).
Van der Lans, R. P., L. T. Pedersen, A. Jensen, K. Glarborg, and K. Dam-Johansen, "Modelling and Experiments of Straw Combustion in a Grate Furnace," *Biomass and Bioenergy*, **19**, 199 (2000).
Van Krevelen, D. W., *Coal, Typology-Physics-Chemistry-Constitution*, Elsevier, 2nd ed. (1981).
Verein Deutscher Ingenieure, ed., *VDI-Wärmeatlas, Berechnungsblätter für den Wärmeübergang*, VDI-Verlag, Düsseldorf, 6th ed. (1991).
Vortmeyer, D., "Radiation in Packed Solids," *German Chem. Eng.*, **3**, 124 (1980).
Winger, F., "Temperatures in a Fuel Particle Burning in a Fluidized Bed: The Effect of Drying, Devolatilization, and Char Combustion," *Combust. and Flame*, **108**, 302 (1997).
Winterberg, M., E. Tsotsas, A. Krischke, and D. Vortmeyer, "A Simple and Coherent Set of Coefficients for Modelling of Heat and Mass Transport with and without Chemical Reaction in Tubes Filled with Spheres," *Chem. Eng. Sci.*, **55**, 967 (1999).

Manuscript received Dec. 5, 2001, and revision received Apr. 22, 2002.